Aerosol retrievals from the EKO MS-711 spectral direct irradiance measurements and corrections of the circumsolar radiation.

Rosa Delia García-Cabrera[1,2], Emilio Cuevas-Agulló[2], África Barreto[3,1,2], Victoria Eugenia Cachorro[1], Mario Pó[4], Ramón Ramos[2], and Kees Hoogendijk[4]

[1]Atmospheric Optics Group, Valladolid University, Valladolid, Spain
[2]Izaña Atmospheric Research Center (IARC), State Meteorological Agency (AEMET), Spain
[3]Cimel Electronique, Paris, France
[4]EKO INSTRUMENTS Europe B.V., The Hague, the Netherlands

Correspondence: Emilio Cuevas Agulló
(ecuevasa@aemet.es)

Abstract. Spectral direct UV-Visible normal solar irradiance (DNI) has been measured with an EKO MS-711 grating spectroradiometer, which has a spectral range of 300-1100 nm, 0.4 nm step, at the Izaña Atmospheric Observatory (IZO, Spain) has been used to determine aerosol optical depth (AOD) at several wavelengths (340, 380, 440, 500, 675 and 870 nm) between April and September 2019 that have been compared with synchronous AOD measurements from a reference Cimel-AERONET (Aerosol RObotic NETwork) sun photometer. The EKO MS-711 has been calibrated at Izaña Observatory using the Langley-Plot method during the study period. Although this instrument has been designed for spectral solar DNI measurements, and therefore has a field of view (FOV) of 5° that is twice that recommended in solar photometry for AOD determination, the AOD differences compared against the AERONET Cimel reference instrument (FOV ∼1.2°), are fairly small. The comparison results between AOD Cimel and EKO MS-711 present a root mean square (RMS) of 0.013 (24.6%) at 340, and 380 nm, and 0.029 (19.5%) for longer wavelengths (440, 500, 675 and 870 nm). However, under relatively high AOD, near forward aerosol scattering might be significant because of the relatively large circumsolar radiation (CSR) due to the large EKO MS-711 FOV, resulting in a small but significant AOD underestimation in the UV range. The AOD differences decrease considerably when CSR corrections, estimated from LibRadtran radiative transfer model simulations, are performed, obtaining RMS of 0.006 (14.9%) at 340 and 380 nm, and 0.005 (11.1%) for longer wavelengths. The percentage of 2- minute synchronous EKO AOD – Cimel AOD differences within the World Meteorological Organization (WMO) traceability limits were ≥ 96% at 500 nm, 675 nm and 870 nm with no CSR corrections. After applying the CSR corrections the percentage of AOD differences within the WMO traceability limits increased to > 95% for 380, 440, 500, 675 and 870 nm, while for 340 nm the percentage of AOD differences showed a poorer increase from 67% to a modest 86%.

1 Introduction

One of the most important elements that governs the Earth's climate, and its processes, is the presence of atmospheric aerosols, which produce a significant radiative forcing resulting from light scattering and absorption, and radiation emission. Moreover,

they act as cloud condensation nuclei, modifying cloud properties (IPCC, 2013). Aerosols effect on the Earth Radiation Balance has been quantified as a cooling of -0.45 W m^{-2}, and -0.9 W m^{-2} when considering the combined effect of both aerosols and clouds. However, the uncertainty of these values is still very high (WMO, 2016), therefore it is necessary to make more efforts to evaluate the aerosol atmospheric content and optical properties, such as the aerosol optical depth (AOD), Ångström exponent (AE), single scattering albedo (SSA), scattering coefficient, and absorption coefficient.

The amount of aerosols present in the atmosphere can be addressed using the aerosol optical depth (AOD) that gives the optical attenuation by aerosols in the atmospheric path. The AOD is derived from surface or satellite observations from sunlight attenuation measurements (WMO, 2016) combined with the Lambert-Beer law. This law has been applied to retrieve the extinction of solar radiation (Ångström, 1930, 1961; Shaw, 1983). The AOD is derived through direct sun radiation measurements at different wavelengths with several instruments such as filter radiometers or spectroradiometers, selecting spectral ranges where the influence of trace gases is minor or even negligible (WMO, 2016; Kazadzis et al., 2018a). The World Meteorological Organization (WMO) recommended the following wavelengths for AOD retrieval: 368, 412, 500, 675, 778 and 862 nm, with a bandwidth of 5 nm (WMO, 1986), and the use of instruments with a full opening angle of 2.5°, and a slope angle of 1° (WMO, 2008).

The AOD retrieval with sunphotometers has been addressed in an extensive list of publications (e.g., Schmid et al. (1999); Kazadzis et al. (2014, 2018a); Barreto et al. (2014); Cuevas et al. (2019)) mainly due to the establishment of aerosol measurement networks, such as AErosol RObotic NETwork (AERONET; Holben et al. (1998)), Precision Filter Radiometer Network (GAW-PFR; Wehrli (2000, 2005)), SKYradiometer NETwork (SKYNET; Takamura and Nakajima (2004)) and SURFace RAdiation Budget Network (SurfRad; Augustine et al. (2008)). Recently, Cuevas et al. (2019) conducted a study comparing AOD from AERONET-Cimel (1.2° field of view (FOV)) with that from GAW-PFR (2.5° FOV) showing a difference of $\sim$3 % at 380 nm and $\sim$2 % at 500 nm compared with AERONET-Cimel for AOD> 0.1, GAW-PFR showing lower values. They demonstrated that this difference was due to the higher amount of dust near-forward scattering measured by GAW-PFR because of it's larger FOV. On the other hand, the AOD retrievals from ground-based spectroradiometers are scarce and normally limited to the visible (VIS) range (e.g. Cachorro et al. (2000); Estellés et al. (2006)). The reason for this shortfall may be found in the high costs in investment and maintenance of spectroradiometers, and their substantial requirements for calibration compared to sun-photometers. However, spectroradiometers offer the possibility to provide other atmospheric components (e.g. O_3, NO_2, SO_2, CH_4 and H_2O) (e.g. Michalsky et al. (1995); Cachorro et al. (1996); Schmid et al. (2001); Barreto et al. (2014); Raptis et al. (2018)).

The first works that attempting to retrieve AOD from spectroradiometers we done by Cachorro et al. (1987) and Ahern et al. (1991), with results based on a few available data. More recently, several works tackled the AOD multi-spectral retrieval from spectroradiometers with larger datasets. Thus, Cachorro et al. (2000) and Vergaz et al. (2005) reported a quantitative characterization of aerosols in Southern Spain. However, they did not provide a comparison with another AOD retrieval method. Kazadzis et al. (2005) and Gröbner et al. (2001) found AOD differences lower than 0.1 at 355 nm and differences between -0.07 and 0.02 at 315.5 316.75 and 320 nm when comparing AOD retrievals performed with Brewer MKIII and Bentham DTM 300 spectroradiometers and Li-cor spectroradiometer, respectively. Estellés et al. (2006) retrieved AOD with a Li-cor

spectroradiometers finding differences with Cimel-318 Sun photometers AOD in the 0.01-0.03 (0.02-0.05) range in the VIS range (UV range). Cachorro et al. (2009) compared AOD retrievals from Li-cor and sunphotometer obtaining AOD differences within 0.02 in the range 440-1200 nm. Kazadzis et al. (2018a) presented the results from the fourth WMO filter radiometer comparison for AOD measurements finding an excellent agreement at 500 and 865 nm between PSR (Precision Solar Spectroradiometer; Raptis et al. (2018)) and PFR (Precision Filter Radiometer; Wehrli (2008)) and overestimation from 0.01 to 0.03, respectively. López-Solano et al. (2018) compared AOD retrievals from Brewer spectroradiometers, AERONET-Cimel and UVPFR in the range 300-320 nm at Izaña Observatory, with uncertainties lower than 0.05.

In this paper we contribute to the knowledge of spectral AOD with a comparison between AOD from AERONET-Cimel sun photometer (onwards, Cimel AOD) and AOD computed from the direct normal irradiance (DNI) measurements performed with an EKO MS-711 spectroradiometer (onwards, EKO AOD). We have also addressed the small, but significant, EKO AOD underestimation under relatively high AOD due to dust near-forward scattering, but in this case have compared two instruments whose FOV values show a big difference since the EKO FOV is 5°. We have divided this work into 5 sections: Sect. 2 describes the main characteristics of the Izaña station and the technical description of the instruments used in this work. In Sect. 3 the methodology used to determine AOD and the corrections due to the differences in dust forward scattering, using the LibRadtran radiative transfer model (RTM) and spectral Langley-Plot calibration are described. In Sect. 4 the main results of the comparison are shown. Finally, a summary and the main conclusions are given in Sect. 5.

2 Site description, Instrument and ancillary information

2.1 Site description

The data used in this work were acquired between April and September 2019 at the Izaña Observatory (IZO). This observatory is located on the island of Tenerife (Spain; 28.3°N, 16.5°W; 2.4 km a.s.l.) and it is approximately 350 km away from the African continent. This observatory is managed by Izaña Atmospheric Research Center (IARC) from the State Meteorological Agency of Spain (AEMET) (more information: http://izana.aemet.es; last access: 7 November 2019).

In 1984, IZO enrolled in the WMO Background Atmospheric Pollution Monitoring Network (BAPMoN) and the WMO Global Atmosphere Watch (GAW) program in 1989. IZO collaborates with different international networks such as the Network for the Detection of Atmospheric Composite Change (NDACC) since 1999, and the GAW-PFR since 2001. In 2003, the Regional Brewer Calibration Centre for Europe (WMO/GAW RBCC-E) was established. Furthermore, IZO has been part of AERONET since 2004, as one of the two AERONET Langley-Plot calibration sites (Toledano et al., 2018). Since 2009, IZO runs a Baseline Surface Radiation Network (BSRN) station. In 2014, IZO was appointed by WMO as a Commission for Instruments and Methods of Observation (CIMO) Testbed for aerosols and water vapor remote sensing instruments (WMO, 2014). More details of IZO programs can be found in Cuevas et al. (2017).

Figure 1. The EKO MS-711 spectroradiometer installed at IZO.

2.2 Instrument: EKO MS-711 spectroradiometer

An EKO MS-711 grating spectroradiometer used in direct sun measurement mode has been tested (Figure 1) within the CIMO Testbed program from April to September 2019 (14706 datapoints).

The EKO MS-711 was designed to measure global solar spectral radiation within the 300 and 1100 nm wavelength range with an average step of $\sim$0.4 nm, exhibiting a full-width-at-half-maximum (FWHM) <7 nm. It is equipped with its own built-in entrance optics, and the housing is temperature-stabilized at 25° $\pm$ 5° (Egli et al., 2016). EKO Instruments designed a collimator tube that also allows measuring DNI (see Figure 1).

This spectroradiometer has been mounted on an EKO sun-tracker STR-21G-S2 (accuracy of <0.01°). This setup performs one spectrum per minute, with an exposure time that changes automatically according to the intensity of the irradiance that varies from 10 ms to 5 s. The main specifications of the EKO MS-711 spectroradiometer are shown in Table 1.

2.3 Ancillary Information: Cimel sun-photometer/AERONET

In this work, we have used AOD data provided by the AERONET permanent Cimel CE318 reference instrument to compare the AOD derived with the EKO MS-711 spectroradiometer. The different Cimel references have been shown to have a good AOD traceability with the GAW-PFR worldwide reference (Cuevas et al., 2019). The world AOD reference is maintained by the World Optical Depth Research and Calibration Center (WORCC) (Kazadzis et al., 2018b).

Table 1. Main specifications of the EKO MS-711 spectroradiometer.

Wavelength range	300 to 1100 nm
Wavelength interval	0.3 - 0.5 nm
Optical resolution FWHM	< 7nm
Wavelength accuracy	$\pm$ 0.2 nm
Cosine response (zenith: 0-80°)	< 5 %
Temp. dependency (-10 °°C to 50 °C)	< 2 %
Temp. control	25 °C $\pm$ 2 °C
Operating temperature	-10 to 50 °C
Exposure time	10 ms^{-5}sec Automatic adjustment
Dome material	Synthetic Quartz Glass
Communication	RS-422 (Between sensor and power supply)
Power requirement	12VDC, 50VA (from the power supply)
Full opening angle (FOV)	5°

The Cimel CE318 photometer is an automatic sun-sky scanning filter radiometer that measures AOD at 340, 380, 440, 500, 675, 870 and 1020 nm (nominal wavelength; extended wavelength versions additionally have 1640 nm) with a full opening angle of 1.2°. The uncertainty in AOD measurements from Cimel field instruments, was estimated to be $\pm$ 0.01 in the VIS range and near-IR, increasing to $\pm$ 0.02 in the UV range (340 and 380 nm) (Eck et al., 1999). This estimate gives an absolute bias < 0.01 for AOD lower than 1.5 (Sinyuk et al., 2012). In this study, we have used AERONET Version 3.0 Level 1.5 AOD data.

3 Methodology

3.1 Spectral Langley Calibration

The EKO MS-711 spectroradiometer was factory calibrated by EKO Instruments making use of a calibrated transfer standard 1000 W quartz tungsten-halogen coiled-coil filament lamp that is traceable to the National Institute of Standards and Technology (NIST) standard (Yoon et al., 2000). The instrument resultant uncertainty is $\pm$ 17% for the UV range, and < 5% for the VIS range. In November 2016, the EKO MS-711 participated in an intercomparison campaign of spectroradiometers at the National Oceanic and Atmospheric Administration (NOAA) Mauna Loa observatory, Hawaii Island, USA (19.54° N, 155.58° W; 3397 m a.s.l.) (Pó et al., 2018), where it was calibrated with the Langley method (Ångström, 1970; Shaw et al., 1973; Shaw, 1983). In 2018 the instrument was deployed at the World Radiation Center- Physical Meteorological Observatory (WRC-PMOD) for its characterization using a tunable laser (Sengupta et al., 2019). Recently, between April and September 2019, the EKO MS-711 has been calibrated at Izaña Observatory using the Langley method in the 300-1100 nm spectral range. In this study we have used the calibration coefficients with the Langley-Plot method.

The Langley method used in the IZO Langley calibration is based on the Beer-Lambert-Bouguer law:

$$DNI(\lambda) = DNI_o(\lambda)e^{-\tau(\lambda)m} \tag{1}$$

where $DNI(\lambda)$ is the direct normal irradiance at wavelength (λ) measured by the instrument, $DNI_o(\lambda)$ is the top-of-atmosphere irradiance corrected for the Sun–Earth distance at wavelength (λ), m is air mass, and $\tau(\lambda)$ is the optical depth tat can be written in the UV-VIS range as:

$$\tau(\lambda) = \tau_R(\lambda) + \tau_a(\lambda) + \tau_{NO_2}(\lambda) + \tau_{H_2O}(\lambda) + \tau_{O_2}(\lambda) + \tau_{O_3}(\lambda) \tag{2}$$

where $\tau_R(\lambda)$ is the Rayleigh optical depth (Hansen and Travis, 1974) due to the molecular scattering that depends on the station pressure as well as on the optical air mass (m_R) (Bodhaine et al., 1999), $\tau_a(\lambda)$ is the AOD, and the rest of the terms are the absorption by atmospheric gases in the affected wavelengths (Gueymard, 2001) and are defined as follows:

$$\tau_R = \frac{P}{P_o} 0.008569\lambda^{-4}(1 + 0.0113\lambda^{-2} + 0.00023\lambda^{-4}) \tag{3}$$

where P is the pressure at the measurement site within the earth's atmosphere, P_o is the standard pressure at sea level and λ is the wavelength in μm. In-situ actual pressure at IZO was used.

$$\tau_{NO_2}(\lambda) = u_{NO_2} A_{NO_2} \tag{4}$$

where u_{NO_2} is the reduced path-length (in atm-cm) taken from the OMI total column NO_2 monthly average climatology and A_{NO_2} its spectral absorption coefficient (Rothman et al., 2013).

$$\tau_{H_2O}(\lambda) = (u_{H_2O} A_{H_2O})^{b_{H2O}} \tag{5}$$

where u_{H_2O} is the column water vapour content (precipitable water) taken from a Global Navigation Satellite System (GNSS) receiver considering satellite precise orbits at IZO (Romero Campos et al., 2009), A_{H_2O} the spectral absorption coefficient Rothman et al. (2013), and the b_{H_2O} exponent depends on the central wavelength position, instrument filter function, as well as the atmosphere pressure and temperature (Halthore et al., 1997). We have determined $\tau_{H_2O}(\lambda)$ from the transmittance for different water vapour and solar zenith angle (SZA) values from the MODTRAN model (Raptis et al., 2018).

$$\tau_{O_2}(\lambda) = (u_{O_2} A_{O_2})^{b_{O2}} \tag{6}$$

where u_{O_2} is the altitude-dependent gaseous scaled path-length taken from the Fourier transform infrared spectrometer (FTIR) measurements at IZO (Schneider et al., 2005), A_{O_2} is the spectral absorption coefficient (Rothman et al., 2013), and the b_{O_2} exponent was obtained from the transmittance values simulated with the MODTRAN model (Berk et al., 2000) for IZO, obtaining a value of 0.454. This value is similar to that obtained by Pierluissi and Tsai (1986, 1987).

$$\tau_{O_3}(\lambda) = u_{O_3} A_{O_3} \tag{7}$$

where u_{O_3} is the total column ozone obtained with a reference Brewer spectrophotometer at IZO (Redondas et al., 2018), and A_{O_3} the ozone absorption cross section (Brion et al., 1993, 1998).

The Langley-Plot determines $DNI_o(\lambda)$ (that allows to derive calibration constant) from a linear extrapolation of $DNI(\lambda)$ measurements to zero air mass, corrected to mean Sun–Earth distance, and plotted on a logarithmic scale versus air mass:

$$lnDNI(\lambda) = lnDNI_o(\lambda) - [\tau_R(\lambda)m_R + \tau_a(\lambda)m_a + \tau_{NO_2}(\lambda)m_{NO_2} + \tau_{H_2O}(\lambda)m_{H_2O} + \tau_{O_2}(\lambda)m_{O_2} + \tau_{O_3}(\lambda)m_{O_3}] \quad (8)$$

where the different air masses have the following expressions:

$$m_R \sim m_{O_2} = \frac{1}{cos(\theta) + 0.50575(96.07995 - \theta)^{-1.6364}}; \text{(Kasten and Young, 1989; Gueymard, 2001)} \quad (9)$$

$$m_a \sim m_{H_2O} = \frac{1}{cos(\theta) + 0.0548(92.65 - \theta)^{-1.452}}; \text{(Kasten, 1966)} \quad (10)$$

$$m_{NO_2} = \frac{1}{sin(\theta) + 602.30(90 - \theta)^{0.5}(27.96 + \theta)^{-3.4536}}; \text{(Gueymard, 1995)} \quad (11)$$

$$m_{O3} = \frac{R + h}{\sqrt{(R + h)^2 - (R + r)^2 sin^2(\theta)}}; \text{(Komhyr et al., 1989)} \quad (12)$$

where R (6370 km) is the mean radius of the Earth, r is the station height above mean see level in km, and h is the mean height of the ozone layer in km (22 km).

3.2 AOD retrieval method

The AOD retrievals have been calculated from Eq. 8, as follows:

$$AOD = \frac{1}{m_a}[lnDNI_o(\lambda) - lnDNI(\lambda) - \tau_R m_R - \tau_{NO_2}(\lambda)m_{NO_2} + \tau_{H_2O}(\lambda)m_{H_2O} + \tau_{O_2}(\lambda)m_{O_2} + \tau_{O_3}(\lambda)m_{O_3}] \quad (13)$$

Grouping the gases contributions such as τ_{gas}, the AOD expression is reduced to:

$$AOD = \frac{1}{m_a}[lnDNI_o(\lambda) - lnDNI(\lambda) - \tau_R m_R - \tau_{gas} m] \quad (14)$$

In this work, we have calculated the EKO AOD at the same nominal wavelengths as those of the Cimel (340, 380, 440, 500, 675 and 870 nm), by integrating the measured irradiance on the considered bandpass (see Table 2), following the methodology used by AERONET (Holben et al. (2001); Giles et al. (2019), and references herein). For each wavelength, we have taken into account the spectral corrections shown in Table 2. All wavelengths have been corrected by the Rayleigh scattering (see Sect. 3.1). Furthermore the 340, 380, 440 and 500 nm are corrected from nitrogen dioxide (NO_2) absorption, being the optical depth calculated using the OMI total column NO_2 climatological monthly averages, and the NO_2 absorption coefficient from Burrows et al. (1999).The 340, 500 and 675 nm channels are corrected of ozone, using the ozone values from the Izaña WMO-GAW reference Brewer spectroradiometer.

Table 2. Wavelengths characteristics of Cimel and spectral corrections used in the calculation of AOD.

Nominal central wavelength (nm)	Filter Bandpass (nm)	Spectral Corrections
340	2	Rayleigh, NO_2, O_3
380	4	Rayleigh, NO_2
440	10	Rayleigh, NO_2
500	10	Rayleigh, NO_2, O_3
675	10	Rayleigh, O_3
870	10	Rayleigh

3.3 Corrections in AOD under relatively high CSR

The full opening angle and the FOV are normally used indistinctly in the literature, which should not be confused with the viewing angle. Therefore, we use the term FOV for referring to the full opening angle. As we remarked in the introduction, the WMO recommended for AOD retrieval the use of instruments with FOV lower than 2.5° and slope angle of 1° (WMO, 2008). As the EKO MS-711 was designed for DNI measurements, it has a larger FOV of 5°, twice the WMO recommended value for AOD retrievals. To account for the different geometries, we have applied a correction to the EKO irradiance measurements. In this section we explain the methodology applied to the measurements and comparisons with Cimel AOD.

The DNI measurement implies that a certain amount of diffuse radiation coming from the line-of-sight of the instrument towards the Sun, and an annular region around it, the so-called circumsolar region, is measured together with the DNI coming from the Sun disk (DNI_{SUN}). The source of this diffuse radiation, CSR (circumsolar radiation), lies on the scattering processes due to the presence of aerosols and clouds (Blanc et al., 2014) in the atmosphere. This CSR has a high dependence on the particle size (Räisänen and Lindfors, 2019), thus large particles (such as desert dust) produce a higher scattering on the incident beam than the smaller particles (e.g., rural background aerosols), leading this contribution to overestimate the DNI. Thus, the experimental DNI measured by a collimated instrument maybe expressed as the sum of both contributions:

$$DNI = DNI_{SUN} + CSR \tag{15}$$

where DNI_{SUN} is the direct normal irradiance coming from the Sun disk and CSR is the diffuse radiation coming from the sky that is seen by the instrument FOV. This FOV is defined by the instrument geometry and determines the amount of CSR reaching the instrument detector. The value of the DNI measured by the instrument also depends on the atmospheric conditions, and the specific instrument characteristics. The most important element that defines the amount of CSR captured by the instrument is the penumbra function *P* (Pastiels, 1959) that defines the fraction of Sun radiation captured or not by the collimator, depending on its angle of vision. This penumbra function can be derived from geometrical features of the instrument (Major, 1980; Blanc et al., 2014): the aperture half-angle α, the slope angle α_s and the limit angle α_l (Fig. 2a). Usually the three angles are known, being the most important the aperture half-angle α. Thus, the radiation coming from the sky with an angle higher than the α_l is outside the collimator and then not measured by the instrument.

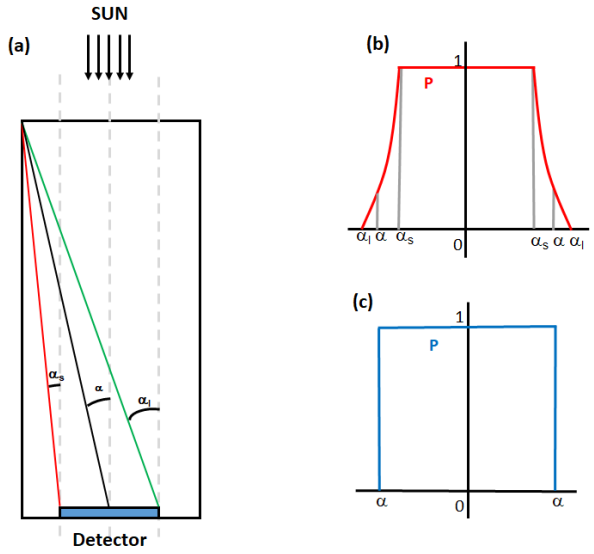

Figure 2. (a) Characteristic angles of the instrument: slope angle α_s, aperture half-angle α and limit angle α_l. On the right, penumbra functions $P(\alpha)$ when (b) the three angles are known and (c) if only the half-angle angle is known. (Figure adapted from Blanc et al. (2014)).

If all angles are known the function P takes the shape of Figure 2b, but if α_s and α_l are unknown, the penumbra function P can be approximated as the shape on Figure 2c. In this work, we used the penumbra function P described in Figure 2c, because α_s and α_l are unknown, and considering that α = FOV/2 = 2.5°.

3.4 CSR simulation

Since it is not possible to obtain accurate CSR measurements, it has been simulated with the LibRadtran radiative transfer model (Mayer and Kylling (2005); Emde et al. (2016), more information http://www.libradtran.org; last access: 7 November 2019), which provides the possibility to simulate the diffuse radiance on sky elements defined by its azimuthal and polar angles. We shortly describe the method followed to simulate the amount of CSR measured by the EKO MS-711. The first step is to describe the geometry of the problem, shown in Figure 3.

For a sky point defined by the polar angle θ and azimutal angle φ, the sky radiance on that point is L (θ,φ) in W m^{-2}sr^{-1}. The angular distance between the considered point and the Sun position (the green arc in Figure 3), is the so-called scattering angle, ξ. To obtain the angle ξ of each point on the sky in terms of the polar and azimuthal angles the next equation should be used:

$$cos(\xi) = cos(SZA)cos(\theta) + sin(SZA)sin(\theta)cos(\varphi - \varphi_{SUN}) \tag{16}$$

Taking into account this relation, the radiation field L can be expressed in terms of ξ and φ, thus the irradiance in the solid angle subtended by an angular distance from the Sun's centre ξ, for an instrument with an aperture half-angle α, is (Blanc et al.,

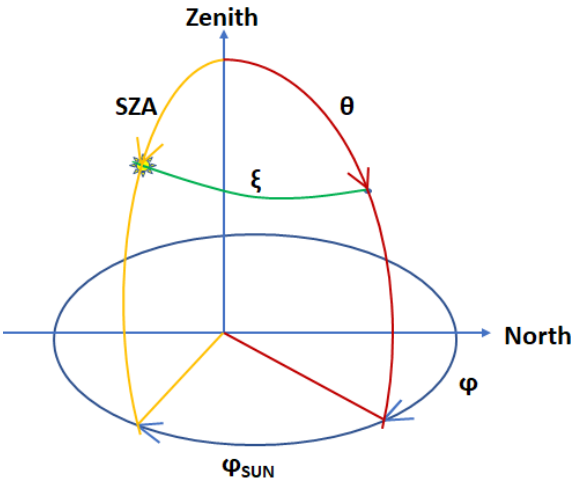

Figure 3. Geometry of the problem. The Sun is located in the coordinates (SZA, $\varphi_{S_{UN}}$) and the sky point is in θ, ϕ. The instrument is located in the origin of the axes.

2014):

$$I = \int_0^{2\pi} \int_{\alpha_o}^{\alpha} P(\xi,\varphi) L(\xi,\varphi) cos(\varphi) sin(\xi) \cdot d\varphi d\xi \tag{17}$$

where $P(\xi,\varphi)$ is the penumbra function defined in Sect. 3.3. If the Sun is in the angular field considered, the obtained irradiance is the DNI of Eq. 15, if not, the result will be only the diffuse radiation. Thus, the key is to simulate the radiances $L(\xi,\varphi)$ of the points in the FOV that the instrument is "seeing". In this work, and taking into account that the instrument is continuously pointing to the Sun, the integration is performed for ξ values from $\alpha_o = 0.6°$ to $\alpha = 2.5°$ with the aim to simulate the diffuse radiation coming from a circumsolar ring, in order to compare AOD from both instruments using the same CSR.

The input parameters used in the simulations are shown in Table 3. The aerosol contribution has been included in the simulations by using the Optical Properties of Aerosols and Clouds (OPAC package) (Hess et al., 1998). This library provides the aerosol (and clouds) optical properties in the range 250 nm to 4000 nm. In our case, we focused the interest in the aerosol mixtures, due to the fact the aerosols in the atmosphere are found as a mixture of different particles. In the LibRadtran package are included the aerosol mixtures described in Hess et al. (1998). The aerosol optical properties stored in the datasets used are: the extinction coefficient, scattering coefficient, absorption coefficient, volume phase function, single scattering albedo and asymmetry parameter. Due to the location of the IZO station we have selected the desert mixtures for the cases of low and high aerosol load.

At this point we should note that the use of 1D simulations with the DISORT (Stamnes et al., 1988) solver implies that the Sun is supposed to be a Dirac function, while, the Sun has an angular radius of 960".12 $\pm$ 0".09 (Emilio et al., 2012). However, Stamnes et al. (1988) demonstrated that the error in DNI_{SUN} simulations, when the Sun is assumed to be a point source,

Table 3. The inputs to LibRadtran model used in this work.

Parameters	Input	Reference
Aerosol parameters	OPAC	Hess et al. (1998)
AOD	AOD estimated from EKO MS-711	-
Altitude	2.4 km	-
Absorption Parameterization	REPTRAN (fine resolution)	Gasteiger et al. (2014)
Atmosphere profile	Midlatitude summer	Anderson et al. (1986)
Solar flux	Kurucz (0.1 nm resolution)	Kurucz (1994)
Slit function	Function Gaussian function with FWHM of 6-7 nm	-
Radiative transfer equation solver	DISORT, with spherical correction for SZA > 60°	Stamnes et al. (1988)
Surface Albedo	0.11	García et al. (2014)
Ozone Column	Ozone column performed with Brewer spectroradiometer at IZO	-
Number of streams	8	-

is negligible with respect to the finite Sun assumption (Stamnes et al., 2000; Reinhardt, 2013) showed that the simulations of radiances in the vicinity of the Sun performed using the DISORT and OPAC aerosols for cloud-free cases give the same result than simulations made with the Monte-Carlo RTE solver MYSTIC included in LibRadtran (Mayer, 2009) taking into account the angular extent of solar disk. The differences remain under 1% and even very close to 0%. Since we want to simulate cloud-free cases, we can use the 1D, DISORT without introducing significant errors in the simulations against the more precise Monte-Carlo simulations.

Once we have selected the input parameters, we must also select the correct angular grid in azimuthal and polar coordinates to cover, at least, the angular region previously defined ($0.6° \leq \alpha \leq 2.5°$). By using Eq. 16 we can calculate the ranges of polar angles and azimuthal angles φ needed. The result of a monochromatic simulation, i.e. $L(\xi, \varphi)$ at 495 nm for the day 26/07/2019 at SZA of $\sim 14°$ is shown in Figure 4a. In Figure 4b the penumbra function, i.e. $P(\xi, \varphi)$ is shown, and in Figure 4c, the result of multiply $P(\xi, \varphi)\ L(\xi, \varphi)$. Note that the angular grid has been selected in steps of 0.1°.

The expected CSR will be obtained by integrating the radiation field $P(\xi, \varphi)\ L(\xi, \varphi)$ as indicated in Eq 17. The integration is done by using the angres tool (Mayer and Kylling, 2005) provided in the LibRadtran package which uses a Monte Carlo integration in 2D to obtain the diffuse radiation in the considered radiation field.

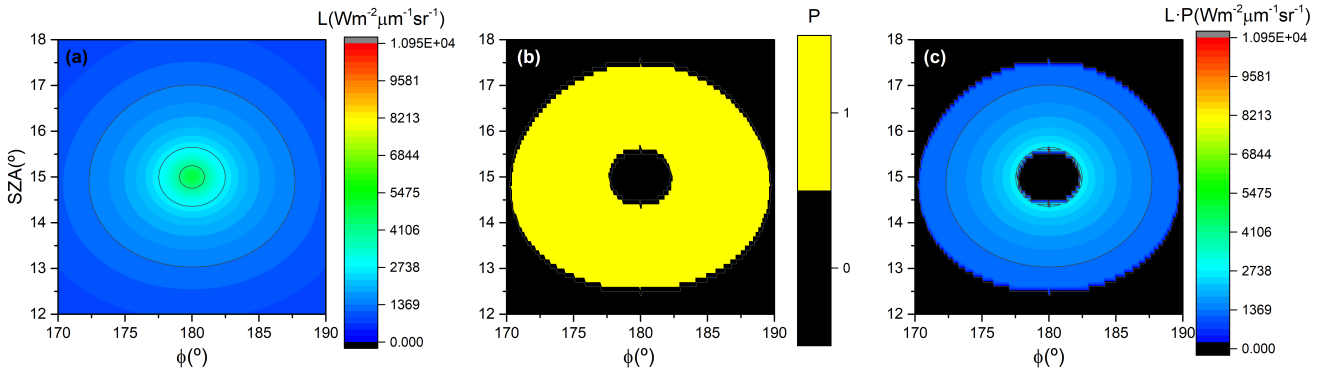

Figure 4. Example of the (a) diffuse radiance L ($\mathrm{Wm}^{-2}\mu m^{-1}\mathrm{sr}^{-1}$) at 500 nm shown in colours at different SZA and φ (b) penumbra function *P* determined from Eq 16 and (c) the product of the diffuse radiance L and penumbra function P.

3.5 AOD retrievals with CSR corrections

Once the CSR has been determined, we apply the correction to the measured DNI taking into account the CSR simulations explained before. Thus, from Eq. 15 the corrected DNI is:

$$DNI_{CORR} = DNI - CSR \tag{18}$$

This correction will lead to a $DNI_{CORR} < DNI$, with which we can retrieve an AOD with a similar expression to Eq. 14:

$$AOD_{CORR} = \frac{1}{m_a}[lnDNI_{oCORR}(\lambda) - lnDNI_{CORR}(\lambda) - \tau_R m_R - \tau_{gas} m] \tag{19}$$

We must note on Eq. 19 that DNI_o, calculated with the Langley-Plot calibration method (see Sec. 3.1), should be also calculated applying a FOV correction using Eq. 8, by substituting DNI_o with the corrected DNI_{oCORR}. The EKO AOD_{CORR} obtained from Eq. 19 with a DNI_{oCORR} calculated from Eq. 18 is supposed to be "free" of any CSR contribution, then it is straight forward to assume that the AOD_{CORR} is closer to the real AOD present in the atmosphere. In order to know the impact of the aerosol load and the FOV size in the values of the CSR simulations we have calculated the ratio of the simulated CSR with respect to the DNI given by Eq. 15, this is the so-called circumsolar ratio (CR) under cloud-free conditions. We have done simulations of DNI_{SUN} and CSR to obtain the previously cited CR, varying the aerosol load in the range [0-0.50] and the FOV in the range [0°–5°]. The rest of the input parameters remain fixed. The results of CR in percentage (Neumann and Witzke, 1999) for a solar zenith angle of 30° is shown for the six Cimel channels in Figure 5.

$$CR(\%) = \frac{CSR}{DNI_{SUN} + CSR} * 100 \tag{20}$$

As can be seen in Figure 5, CR increases for higher FOV and larger AOD, as expected, and for the lower wavelengths. The dashed lines in Figure 5 indicate the FOV of the instruments used in this work Cimel (blue line) and EKO (red line). The CR

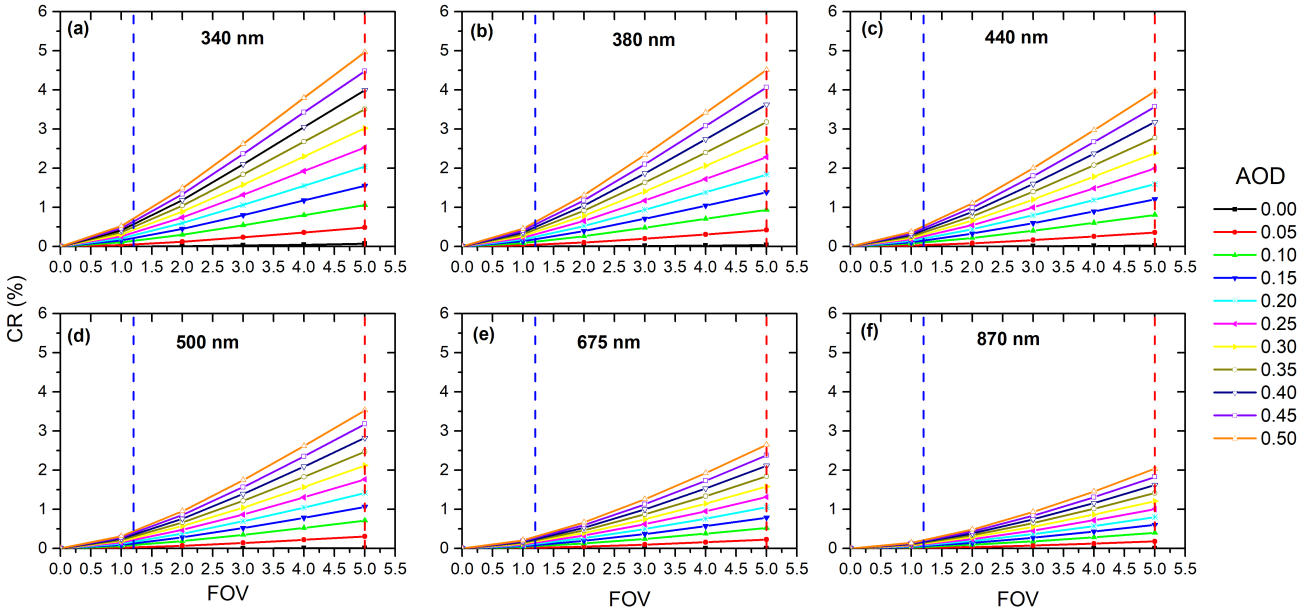

Figure 5. Simulations of CR at (a) 340, (b) 380, (c) 440, (d) 500, (e) 675 and (f) 870 nm for AOD between 0.0 and 0.50 and FOV between 0° and 5° at SZA 30°. The dashed blue and red lines represent the Cimel FOV (1.2°) and EKO MS-711 FOV (5°), respectively.

for the Cimel in all cases is lower than 1% and even 0.5% for the channels over 440 nm. For EKO the CR ranges between 2% in the 870 nm channel and 5% for the 340 nm channel. Thus, the expected CSR maximum values in Figure 5 should be found at these conditions: FOV of 5°, AOD of 0.50 and wavelength of 340 nm, in which a CR of 5% is found. We have simulated the AOD retrievals as a function of CSR. By combining Eq. 18 to 20, we can vary CR (in fact the value of CSR) and calculate the AOD retrieved with the corresponding DNI_{oCORR}.

These results indicate that the CSR impacts significantly on the EKO AOD retrievals under relatively high AOD leading to AOD underestimation, with this effect being less important for the Cimel AOD retrievals because of its narrower FOV.

These results have been simulated considering the typical conditions of IZO where mineral dust is practically the only aerosol present (Berjón et al., 2019; García et al., 2017). Simulations of the effect on CR of the eight OPAC mixture aerosols available in LibRadtran model, continental (clean, average and polluted), urban, maritime (clean, polluted and tropical) and desert aerosols (Hess et al., 1998), and for a FOV=5°, are shown in Figure 6. For SZA=30°, with an AOD_{500nm} range between 0 and 2 at sea level, two defined groups are distinguished: the continental and urban aerosol mixtures, and the maritime and desert dust mixtures. It should be noted that for stations located in urban or continental (clean and contaminated) environments, which are the majority, the correction that would have to be made to the AOD for a very high aerosol load (e.g., AOD = 1) would be much lower, between 1/3 to 1/6, than the correction that would have been performed in the case of dust aerosol. (Figure 6 and Appendix B).

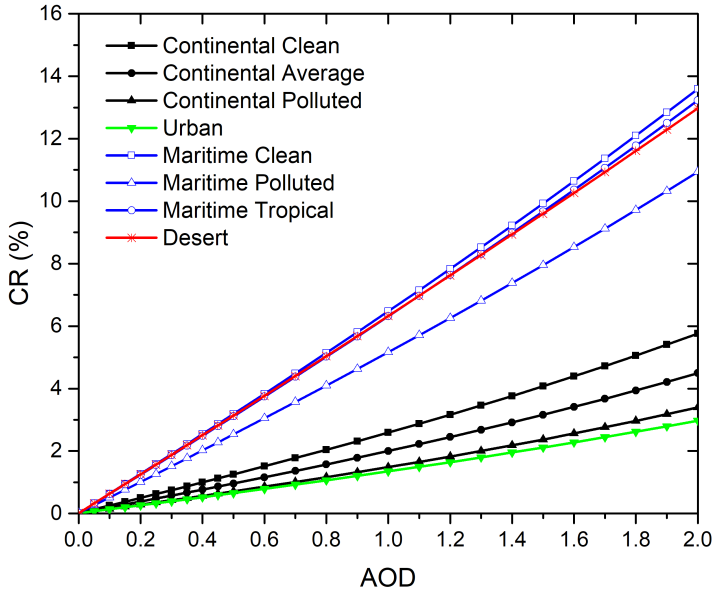

Figure 6. Simulations of CR (%) for SZA 30° at sea level for AOD values between 0 and 2, at 500 nm, for different types of aerosols for FOV of 5°.

4 Results

4.1 Langley calibration at Izaña Observatory

Based on the experience of Kiedron and Michalsky (2016) and Toledano et al. (2018), we have considered that the Langley calibration is suitable if the standard deviation (σ) of the fit (Eq. 8) is lower than 0.006, the correlation coefficient (R) > -0.99, the number of valid points > 33% of the initial sample, and AOD (500 nm) < 0.025. In order to test the Langley method described in Sect. 3.1, an example of Langley-Plots using the UV-VIS-near IR direct-Sun measurements on 19 March 2019 at Izaña Observatory are shown in Figure 7.

The comparison between the factory calibration performed by EKO Instruments in 2016 and the IZO Langley-Plot calibration (2019) is shown in Figure 8. These results indicate that the stability of the EKO MS-711 in the range 300-1100 nm during a 3 years period, between the manufacturer lamp calibration and the Langley calibrations at IZO, is remarkable. The factory calibration and the IZO Langley-Plot calibration three years later present differences $\sim$ 4.8% between 350 and 1100 nm and even $\leq$ 2.3% and 3.1% in the VIS and near-IR range, respectively. The larger differences below 350 nm are attributed to the low halogen lamp signal in this region experienced during the factory calibration, and low instrument sensitivity in this region.

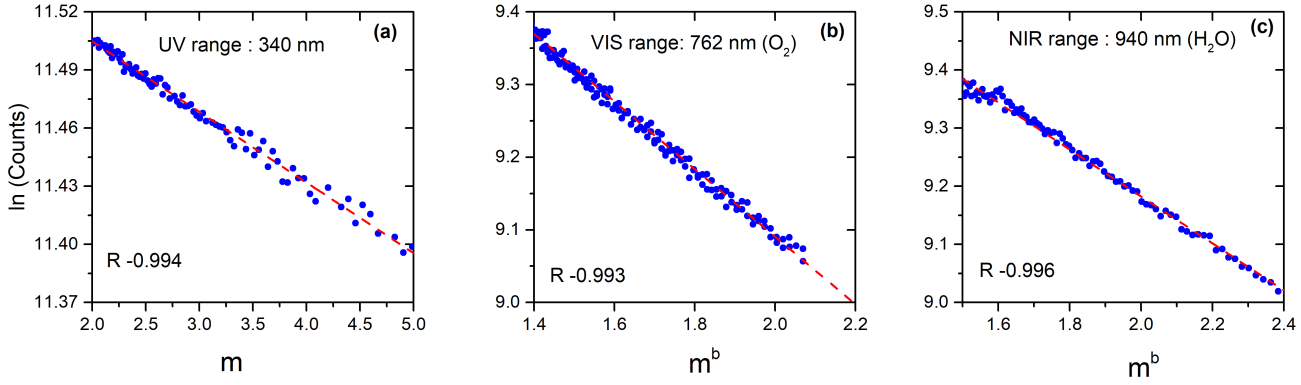

Figure 7. Examples of Langley-Plots using the UV-VIS-near IR direct-Sun measurements on 19 March 2019 at Izaña Observatory at (a) 340 nm, (b) 762 nm (O2) and (c) 940 nm (H2O) nm. R: correlation coefficient.

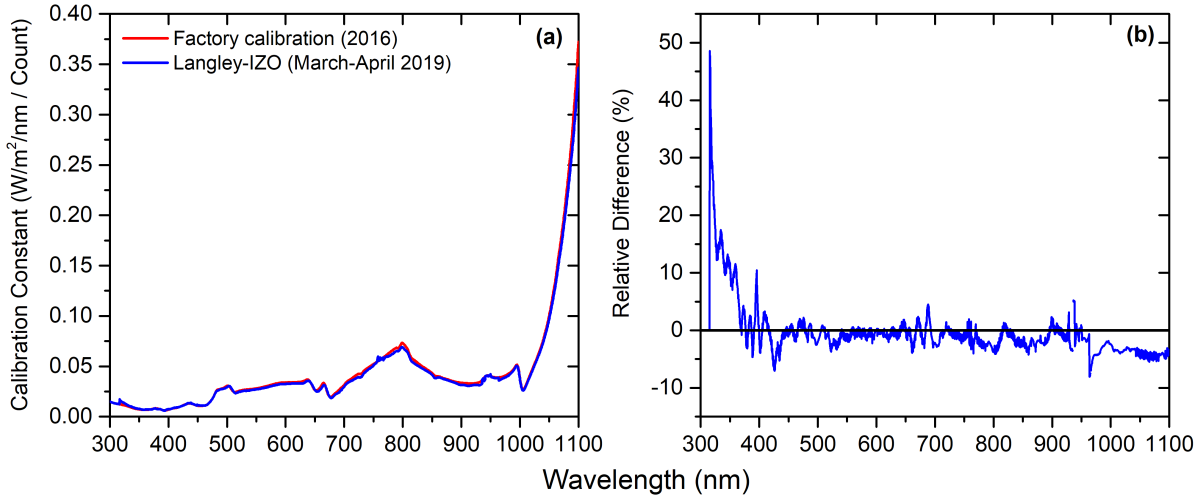

Figure 8. (a) Calibration constants (W m^{-2}/nm/Count) of the EKO MS-711 spectroradiometer, and (b) relative differences between factory calibration constants and those obtained from Langley-Plots at IZO.

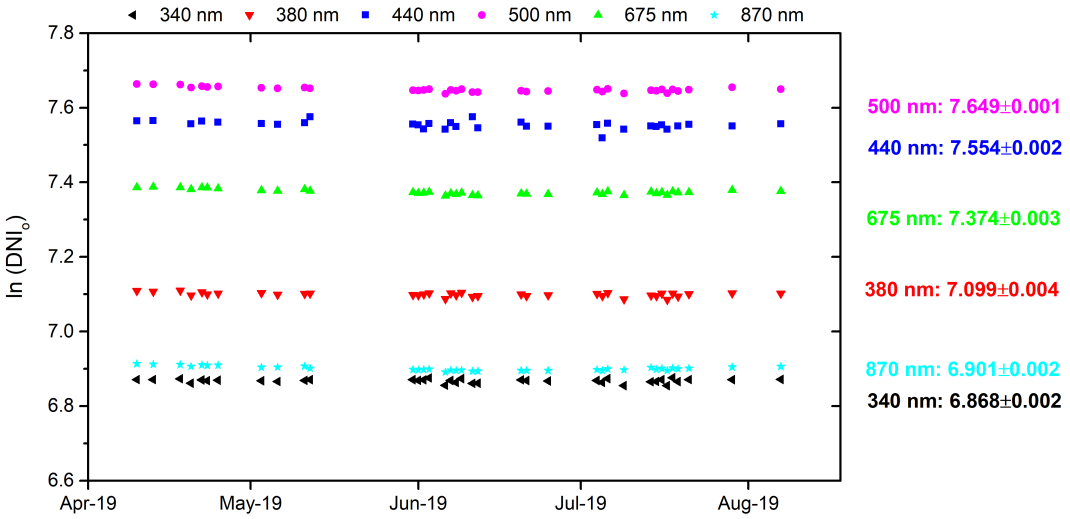

Figure 9. EKO MS-711 *DNI$_o$(λ)* values, and corresponding standard deviations, between April and September 2019 at IZO, for all nominal wavelengths measured by the Cimel (340, 380, 440, 500, 675 and 870 nm).

Applying the previous method, $DNI_o(\lambda)$ values and their standard deviations from the EKO MS-711 measurements (from April to September 2019 at Izaña Observatory) at the nominal wavelengths measured by the Cimel (340, 380, 440, 500, 675 and 870 nm), as a function of time are shown in Figure 9. These $DNI_o(\lambda)$ values have been used in the AOD retrievals.

4.1.1 AOD retrievals

In this section, we present the results obtained when comparing Cimel AOD and EKO AOD with no CSR corrections (CSR uncorrected AOD) and applying a CSR correction (CSR corrected AOD). The comparisons were done considering measurements of both instruments that match within 2 minutes for all wavelengths. This approach produced a Cimel and EKO AOD dataset with a total of 14706 quasi-coincident measurements. The results show (Table 4) that there is a good agreement (correlation coefficient > 0.98) between EKO AOD and Cimel AOD for all channels, even for no CSR correction, except for the lowest 340 nm UV channel.

The uncorrected EKO AOD shows slopes ∼1.06 and correlation coefficients over 0.97 for all wavelengths. The RMS ranges from 0.017 (28.9%) at 340 nm to 0.004 (18.8%) at 870 nm. These results improve significantly when taking into account the CSR corrections for all wavelengths. Thus, for the corrected EKO AOD the correlation coefficients are ∼0.98 for the shorter wavelengths and ∼1 for the rest of the wavelengths. The RMS and MB show the same trend as that for the uncorrected EKO AOD case, that is, we find the lowest values for the higher wavelengths. The negative values of the MB (EKO AOD – Cimel

Table 4. Statistics of the comparison between EKO AOD, with no CSR corrections (CSR Unc.) and implementing CSR corrections (CSR Corr.), and Cimel AOD at 340, 380, 440, 500, 675 and 870 nm at IZO between April and September 2019. R: correlation coefficient, slope of the least-squares fit between EKO AOD and Cimel AOD, RMS: root mean square of the bias and MB: mean bias. The results of the relative bias are in brackets (in %).

Wavelength	**R**		**Slope**		**RMS**		**MB**	
(nm)	**CSR Unc.**	**CSR Corr.**	**CSR Unc.**	**CSR Corr.**	**CSR Unc.**	**CSR Corr.**	**CSR Unc.**	**CSR Corr.**
340 nm	0.960	0.973	1.063	0.994	0.017	0.007	0.015	<0.001
					(28.9%)	(16.9%)	(24.5%)	(-1.4%)
380 nm	0.981	0.986	1.071	1.001	0.009	0.005	0.007	<0.001
					(20.2%)	(12.9%)	(14.8%)	(1.2%)
UV-Range (Mean)	0.971	0.979	1.067	0.997	0.013	0.006	0.011	<0.001
					(24.6%)	(14.9%)	(19.7%)	(1.3%)
440 nm	0.984	0.987	1.041	0.997	0.101	0.005	0.009	0.001
					(22.4%)	(13.5%)	(18.7%)	(0.6%)
500 nm	0.988	0.991	1.075	1.018	0.007	0.005	0.004	0.002
					(18.2%)	(12.9%)	(12.1%)	(0.4%)
675 nm	0.989	0.991	1.057	1.013	0.006	0.006	0.003	<0.001
					(19.7%)	(10.7%)	(11.2%)	(0.5%)
870 nm	0.998	0.999	1.039	1.009	0.004	0.003	<0.001	<0.001
					(18.8%)	(7.3%)	(0.3%)	(0.2%)
VIS-Range (Mean)	0.989	0.992	1.053	1.009	0.029	0.005	0.004	<0.001
					(19.5%)	(11.1%)	(10.6%)	(0.4%)

AOD), indicate that the EKO AOD values are normally lower than the Cimel AOD values. However, these values are within the Cimel instrument uncertainties, $\pm$0.01 in the VIS and near-IR and $\pm$0.02 in the UV ranges (Eck et al., 1999). These results also agree with other studies. For example, Estellés et al. (2006) and Cachorro et al. (2009) found differences between 0.01 and 0.03 in the VIS range, and between 0.02 and 0.05 for the UV when comparing Li-cor AOD with Cimel AOD. Recently, Kazadzis et al. (2018a) found AOD differences ranging between 0.01 and 0.03 at 500 and 865 nm, respectively, when comparing AOD from PSR and PFR. Recently, Cuevas et al. (2019), using long-term AOD data series from both GAW-PFR and AERONET-Cimel radiometers reported differences in AOD $\sim$3% lower at 380 nm and $\sim$2% lower at 500 nm for GAW-PFR due to its larger FOV.

The box plots of MB differences (EKO AOD – Cimel AOD) for different AOD intervals are presented in Figure 10. In general, it can be seen that a significant improvement in the AOD retrievals is found after CSR correction, with the corrected AOD medians being closer to 0 in all wavelengths. The improvement in AOD for AOD>0.1 conditions (20% of the data for 340 and 380 nm, and 16% for the rest of the wavelengths) is remarkable, as already mentioned in the CSR correction section.

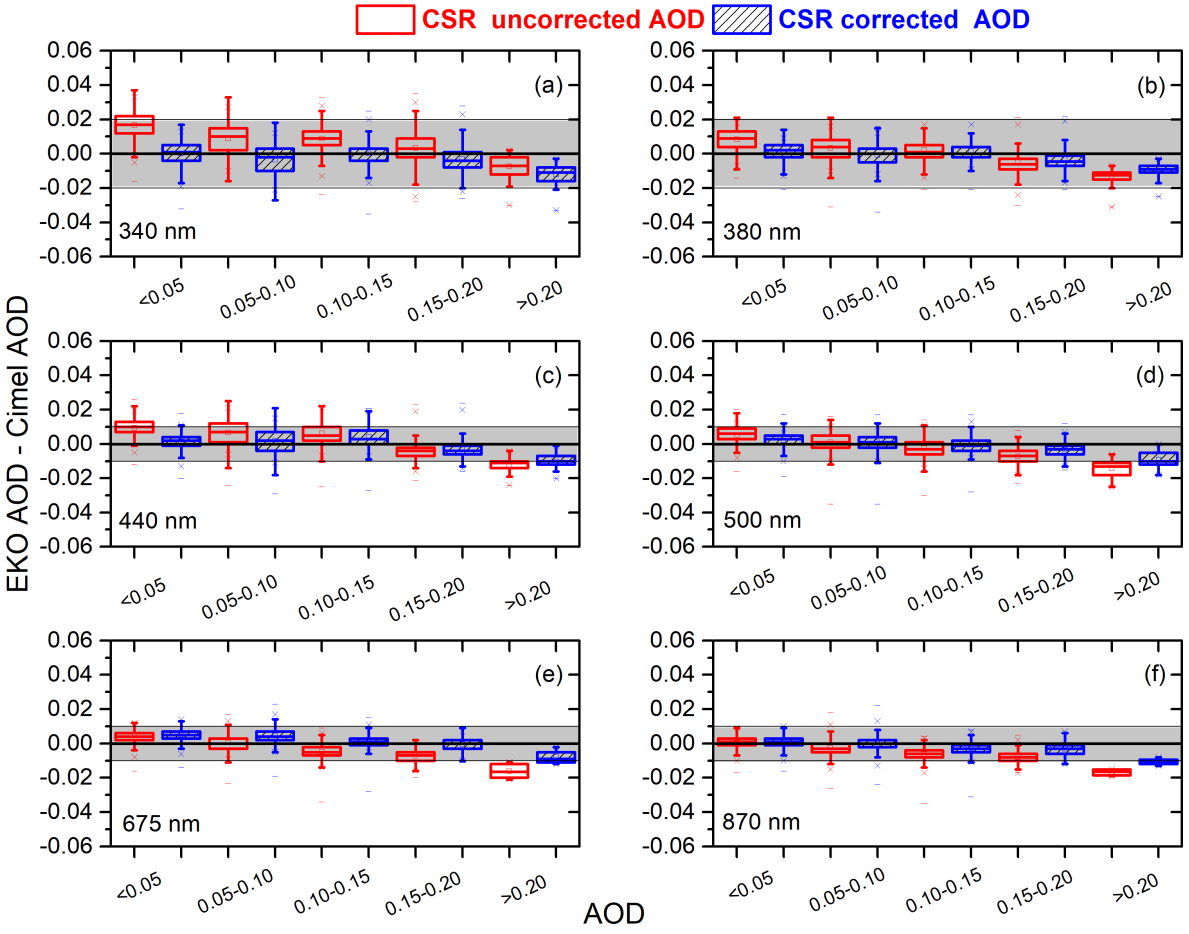

Figure 10. Box plot of the differences between the EKO AOD with (no) CSR corrections, and Cimel AOD versus AOD for the period April-September 2019 at IZO in blue (red). Lower and upper boundaries for each box are the 25^{th} and 75^{th} percentiles; the solid line is the median value; the crosses indicate values out of the 1.5-fold box area (outliers); and hyphens are the maximum and minimum values. Shadings show the range of uncertainty of Cimel (±0.02 for the UV range and ±0.01 for VIS and near-IR ranges; Eck et al. (1999)).

Table 5. Linear AOD-correction equations (slope and intercept) at 340, 380, 440, 500, 675 and 870 nm obtained with data measured from April 1st to July 31^{st} 2019 at Izaña Observatory. Validation of the linear AOD-correction equations was performed using data obtained between August 1^{st} and September 30^{th} 2019.

	Linear AOD-correction Equations: Corrected EKO AOD = Slope*EKO AOD + Intercept 01/04/2019-31/07/2019			**Validation 01/08/2019-30/09/2019**		
Wavelength (nm)	**Slope**	**Intercept**	**R**	**RMS**	**MB**	**R**
340	1.076	-0.019	0.997	0.005 (5.9%)	-0.003 (-4.0%)	0.998
380	1.073	-0.0102	0.999	0.003 (2.9%)	-0.003 (-1.6%)	0.999
440	1.066	<0.001	0.999	0.002 (2.4%)	<0.001 (-1.2%)	0.999
500	1.056	-0.005	0.999	0.002 (2.9%)	-0.001 (-2.1%)	0.999
675	1.043	0.003	0.999	0.001 (2.4%)	<0.001 (-1.7%)	0.999
870	1.031	<0.001	0.999	<0.001 (1.4%)	<0.001 (-0.02%)	0.999

The scatter is also significantly reduced for all wavelengths and aerosol loads, except in the 340 nm UV channel. This is mainly attributed to the instrumental error in the spectral range between 300 and 350 nm (17.2%), of which 6% corresponds to stray-light and 6% corresponds to measurement repeatability (Zong et al., 2006), to the different FWHM between EKO (7 nm) and CIMEL (2 nm) at 340 nm, and to the fact that Rayleigh and aerosol scattering are higher in the UV range (Cuevas et al., 2019). Despite these drawbacks, the improvement in AOD is significant performing a simple correction of the CSR estimated with LibRadtran.

The linear AOD-correction equations were determined by using data measured from April 1^{st} to July 31^{th} 2019 (69% of the data) at Izaña Observatory (Table 5). The validation of these linear AOD-correction equations was performed using an independent period of data (between August 1st and September 30^{th} 2019; 31% of the data). Note that abs(MB) $\leq$1.6% for all wavelengths except for 340 nm for which a significantly larger MB (-4.0%) is registered. In any case it should be noted that the CSR correction applied in this study has been made under the presence of mineral dust. It would be necessary to verify that these CRS corrections have similar validity under moderate-high influence of other types of aerosols, such as marine or biomass burning aerosols.

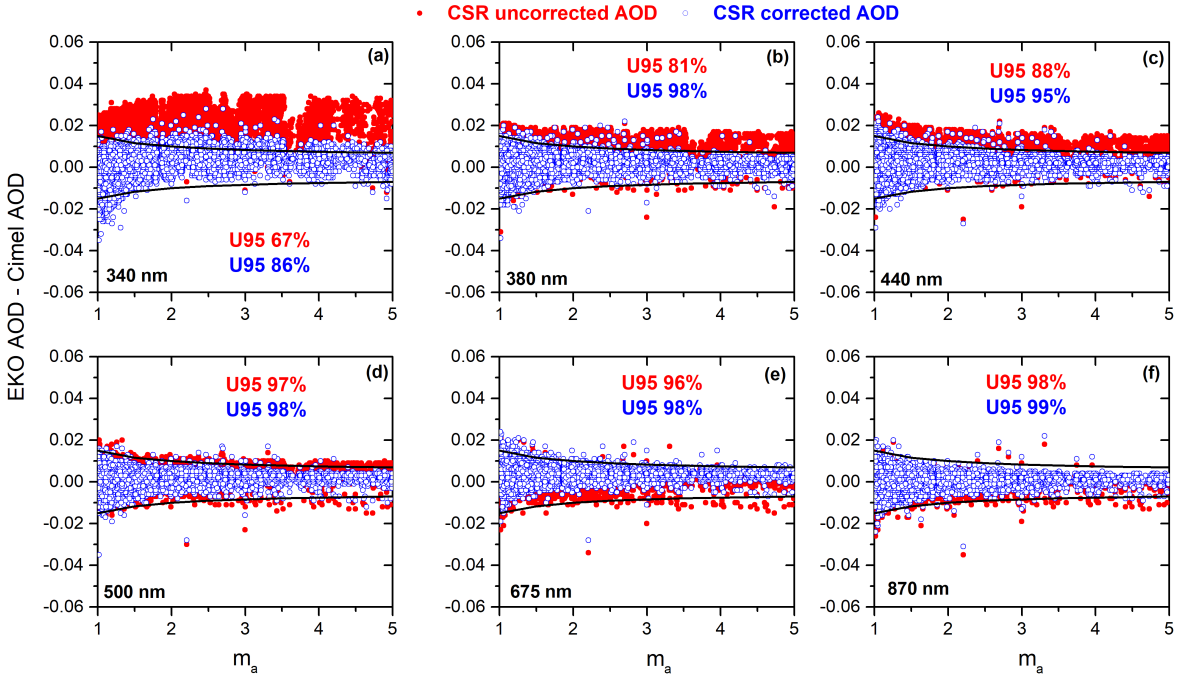

Figure 11. AOD differences (EKO AOD – Cimel AOD) versus the optical air mass (m_a). Black lines represent the U_{95} uncertainty limits.

In order to check the quality of EKO AOD, we have applied the WMO traceability criteria (WMO, 2005) defined for finite FOV instruments as:

$$U_{95} = \pm(0.005 + 0.010 m_a) \tag{21}$$

where m_a is the optical air mass. The percentage of data meeting the WMO traceability requirements (95% of the AOD differences of an instrument compared to the WMO standards lie within specific limits) is > 95% at 500, 675 and 870 nm, taking the AERONET-Cimel as the reference (Figure 11).

The percentage of EKO AOD data meeting the WMO criteria increases considerably when we take into account the CSR corrections, increasing from 67% to more than 86% at 340 nm, and above 95% for the rest of the channels. The poorest results shown by the 340 nm channel (86%), might be partially explained by the. EKO's 7nm FWHM influence on the smaller 2 and 4nm band pass UV channels. The instrument uncertainty is larger in the UV range, which is mostly associated with stray-light in the instrument inner optics (Zong et al., 2006).

When focusing the analysis on relatively high AOD (AOD> 0.10), we found that the percentage of AOD differences out of the WMO U_{95} limits were ~3.5% (0.8% of the data) at 380 nm and 0.6% (0.3% of the data) at 870 nm, consistent with the lower percentages of AOD differences out of the WMO U_{95} reported by Cuevas et al. (2019) when comparing GAW-PFR (FOV $\sim 2.5°$) and AERONET-Cimel radiometers that present a lower difference in FOV (1.2°).

5 Conclusions

In this work, we present the characterization of an EKO MS-711 spectroradiometer. The instrument has been calibrated at Izaña Observatory using the Langley-Plot method between April and September 2019. This calibration has been compared with the lamp calibration performed at EKO Instruments factory in 2016, obtaining relative differences $\leq$2.3% and 3.1% in the VIS and near IR range, respectively. These results indicate a high spectral stability of the instrument in this 3-year time period (2016-2019).

The EKO MS-711 has been designed for spectral solar DNI measurements, and therefore it has a relatively high FOV (5°), double the FOV recommended by WMO for AOD radiometers, and four times larger than the AERONET-Cimel FOV. This difference in FOV might lead to a significant difference in near forward scattering under relatively high aerosol content, resulting in a small, but significant, AOD underestimation, especially in the UV range.

However, the AOD retrievals from an EKO MS-711 spectral DNI measurements show a rather good agreement with those from an AERONET reference radiometer. The AOD comparison was held at Izaña Observatory between April and September 2019. Quality assessment of the EKO MS-711 AOD has been performed by comparing with coincident AOD from AERONET at 340, 380, 440, 500, 675 and 870 nm considering measurements of both instruments as close as 2 minutes between them, with a total of 14706 analyzed data-pairs. The skill scores of the AOD comparison are fairly good with a RMS of 0.013 (24.6%) at 340 and 380 nm, and 0.029 (19.5%) for longer wavelengths (440, 500, 675 and 870 nm), with AOD being underestimated by the EKO radiometer. The MB (EKO AOD – Cimel AOD) are 0.011 (19.7%) for 340 and 380 nm and 0.004 (10.6%) for 440, 500, 675 and 870 nm. These results improve considerably when we take into account the CSR corrections to EKO AOD because of the higher EKO FOV. The CSR differences between EKO and AERONET-Cimel were obtained using LibRadtran model. When comparing EKO AOD corrected values the RMS is reduced to 0.006 (14.9%) at 340 and 380 nm, and to 0.005 (11.1%) for longer wavelengths, while MB is reduced to <0.001 (1.3%) for 340 and 380 nm, and <0.001 (0.4%) for 500, 675 and 870 nm. These values are within the Cimel instrumental uncertainty ($\pm$0.01 in the VIS and near-IR, and $\pm$0.02 in the UV ranges).

Following WMO recommendations we have analysed the percentage of EKO AOD – Cimel AOD differences within WMO U_{95} limits defined for finite FOV instruments, we found that with no CSR-corrections $\geq$96% of the AOD differences fell within the WMO U_{95} limits at 500, 675 and 870 nm. After applying the CSR-corrections, the percentage of AOD differences within the WMO U_{95} limits were >95% for 380, 440, 500, 675 and 870 nm, while for 340 nm the percentage of AOD differences within the WMO U_{95} increased only to a modest 86%. The known greater AOD uncertainty in the UV range along with stray-light problems not fully corrected in this instrument seem to be behind the poorer AOD agreement with AERONET-Cimel at 340 nm.

The EKO-MS711 has proven to be an instrument, which despite having been designed for solar radiation measurements, can provide high quality AOD measurements in the VIS and near-IR ranges with excellent results when compared with the AERONET-Cimel reference radiometer, which, in turn has shown a very good AOD traceability with the WORCC AOD world reference.

Data availability. The Cimel-AERONET data from the Izaña station ("Izana") are available from the AERONET website: https://aeronet.gsfc.nasa.gov/ (last access: 14 November 2019). The EKO MS-711 data might be available upon request to EKO Instruments and Izana WMO CIMO Testbed.

Author contributions. RDG and EC designed the structure and methodology of the paper and wrote the main part of the manuscript. RDG computed all the calculations performed in the paper. AB discussed the modelling results and participated in the AOD retrieval and the Langley calibration analysis. VEC provided interesting ideas used in this paper, and advice based on her experience in spectroradiometry. RR performed the maintenance and daily checks of the EKO-MS711 spectroradiometer. MP provided detailed technical information and calibrations of the EKO-MS711 spectroradiometer. KH allowed that the EKO-MS711 used in this study could be evaluated in the WMO CIMO Izaña testbed taking care of all the associated logistics. All authors discussed the results and contributed to the final paper.

Competing interests. The authors declare that they have no conflict of interest.

Acknowledgements. This work has been developed within the framework of the activities of the World Meteorological Organization (WMO) Commission for Instruments and Methods of Observation (CIMO) Izaña test bed for aerosols and water vapor remote sensing instruments. The authors are grateful to EKO Instruments for its availability that the EKO-MS711 spectroradiometer has been tested and evaluated independently by the WMO CIMO Izaña testbed. The LibRadtran Radiative Transfer Model has been used to estimate the circumsolar radiation. AERONET Sun photometers at Izaña have been calibrated within the AERONET Europe TNA, supported by the European Union Horizon 2020 research and innovation program under grant agreement no. 654109 (ACTRIS-2). This research benefited from the results of the project funding by MINECO RTI2018-097864-B-I00. We also acknowledge our colleague Celia Milford for improving the English of the manuscript.

Appendix A:

Abbreviations

AEMET State Meteorological Agency of Spain

AERONET AErosol RObotic NETwork

AOD Aerosol Optical Depth

BapMon Background Atmospheric Pollution Monitoring Network

BSRN Baseline Surface Radiation Network

CIMO Commission for Instruments and Methods of Observation

CSR Circumsolar Radiation

DNI Direct Normal Irradiance

FOV Field of View

FTIR Fourier Transform Infrared Spectrometer

FWHM Full Width at Half Maximum

GAW-PFR Precision Filter Radiometer Network

GNSS Global Navigation Satellite System

IARC Izaña Atmospheric Research Center

IZO Izaña Observatory

MB Mean Bias

NDACC Network for the Detection of Atmospheric Composite Change

NIST National Institute of Standards and Technology

NOAA National Oceanic and Atmospheric Administration

OPAC Optical Properties of Aerosols and Clouds

PSR Precision Solar Spectroradiometer

RMS Root Mean Square

SKYNET SKYradiometer NETwork

SURFRAD SURFace RADiation Budget Network

SZA Solar Zenith Angle

UV Ultraviolet Range

VIS Visible Range

WMO World Meteorological Organization

WORCC World OpticalDepth Research and Calibration Center

WRC-PMOD World Radiation Center- Physical Meteorological Observatory

Appendix B:

Numerical values of the CR (%) simulations for SZA 30° at sea level for AOD values between 0 and 2, at 500 nm, for different types of aerosols for FOV of 5°.

AOD	Continental Clean	Continental Average	Continental Pollution	Urban	Maritime Clean	Maritime Pollution	Maritime Tropical	Desert
	CR (%)	CR (%)	CR (%)	CR (%)	CR (%)	CR (%)	CR (%)	CR (%)
0.1	0.3	0.2	0.1	0.1	0.6	0.5	0.6	0.6
0.2	0.5	0.4	0.3	0.3	1.3	1.0	1.2	1.3
0.3	0.7	0.6	0.4	0.4	1.9	1.5	1.9	1.9
0.4	1.0	0.8	0.6	0.5	2.5	2.0	2.5	2.5
0.5	1.3	1.0	0.7	0.7	3.2	2.5	3.1	3.1
0.6	1.5	1.2	0.9	0.8	3.8	3.1	3.7	3.8
0.7	1.8	1.4	1.0	0.9	4.5	3.6	4.4	4.4
0.8	2.0	1.6	1.2	1.1	5.1	4.1	5.0	5.0
0.9	2.3	1.8	1.3	1.2	5.8	4.6	5.7	5.7
1	2.6	2.0	1.5	1.3	6.5	5.2	6.3	6.3
1.1	2.9	2.2	1.7	1.5	7.1	5.7	7.0	7.0
1.2	3.2	2.4	1.8	1.6	7.8	6.3	7.6	7.6
1.3	3.5	2.7	2.0	1.8	8.5	6.8	8.3	8.3
1.4	3.8	2.9	2.2	2.0	9.2	7.4	9.0	8.9
1.5	4.1	3.2	2.4	2.1	9.9	8.0	9.7	9.6
1.6	4.4	3.4	2.6	2.3	10.6	8.5	10.4	10.3
1.7	4.7	3.7	2.8	2.4	11.4	9.1	11.1	10.9
1.8	5.1	3.9	3.0	2.6	12.1	9.7	11.8	11.6
1.9	5.4	4.2	3.2	2.8	12.8	10.3	12.5	12.3
2	5.8	4.5	3.4	3.0	13.6	10.9	13.2	13.0

References

Ahern, F. J., Gauthier, R. P., Teillet, P. M., Sirois, J., Fedosejevs, G., and Lorente, D.: Investigation of continental aerosols with high-spectral-resolution solar-extinction measurements, Appl. Opt., 30, 5276–5287, https://doi.org/10.1364/AO.30.005276, 1991.

Anderson, G., Clough, S., Kneizys, F., Chetwynd, J., and Shettle, E.: AFGL atmospheric constituent profiles, Environ. Res. Pap, 954, 1–46, 1986.

Ångström, A.: On the atmospheric transmission of sun radiation. II, Geografiska Annaler, 12, 130–159, 1930.

Ångström, A.: Techniques of determinig the turbidity of the atmosphere, Tellus, 13, 214–223, 1961.

Ångström, A.: Apparent solar constant variations and their relation to the variability of atmospheric transmission, Tellus, 22, 205–218, https://doi.org/https://doi.org/10.1111/j.2153-3490.1970.tb01522.x, 1970.

Augustine, J. A., Hodges, G. B., Dutton, E. G., Michalsky, J. J., and Cornwall, C. R.: An aerosol optical depth climatology for NOAA's national surface radiation budget network (SURFRAD), Journal of Geophysical Research: Atmospheres, 113, https://doi.org/10.1029/2007JD009504, 2008.

Barreto, A., Cuevas, E., Pallé, P., Romero, P. M., Guirado, C., Wehrli, C. J., and Almansa, F.: Recovering long-term aerosol optical depth series (1976-2012) from an astronomical potassium-based resonance scattering spectrometer, Atmospheric Measurement Techniques, 7, 4103–4116, https://doi.org/10.5194/amt-7-4103-2014, 2014.

Berjón, A., Barreto, A., Hernández, Y., Yela, M., Toledano, C., and Cuevas, E.: A 10-year characterization of the Saharan Air Layer lidar ratio in the subtropical North Atlantic, Atmospheric Chemistry and Physics, 19, 6331–6349, https://doi.org/10.5194/acp-19-6331-2019, https://www.atmos-chem-phys.net/19/6331/2019/, 2019.

Berk, A., Acharya, P. K., Bernstein, L. S., Anderson, G. P., Chetwynd Jr, J. H., and Hoke, M. L.: Reformulation of the MODTRAN band model for higher spectral resolution, in: Algorithms for Multispectral, Hyperspectral, and Ultraspectral Imagery VI, vol. 4049, pp. 190–198, International Society for Optics and Photonics, https://doi.org/https://doi.org/10.1117/12.410340, 2000.

Blanc, P., Espinar, B., Geuder, N., Gueymard, C., Meyer, R., Pitz-Paal, R., Reinhardt, B., Renné, D., Sengupta, M., Wald, L., and Wilbert, S.: Direct normal irradiance related definitions and applications: The circumsolar issue, Solar Energy, 110, 561 – 577, https://doi.org/https://doi.org/10.1016/j.solener.2014.10.001, 2014.

Bodhaine, B. A., Wood, N. B., Dutton, E. G., and Slusser, J. R.: On Rayleigh optical depth calculations, Journal of Atmospheric and Oceanic Technology, 16, 1854–1861, 1999.

Brion, J., Chakir, A., Daumont, D., Malicet, J., and Parisse, C.: High-resolution laboratory absorption cross section of O3. Temperature effect, Chemical physics letters, 213, 610–612, 1993.

Brion, J., Chakir, A., Charbonnier, J., Daumont, D., Parisse, C., and Malicet, J.: Absorption spectra measurements for the ozone molecule in the 350–830 nm region, Journal of atmospheric chemistry, 30, 291–299, 1998.

Burrows, J., Richter, A., Dehn, A., Deters, B., Himmelmann, S., Voigt, S., and Orphal, J.: Atmospheric remote-sensing reference data from GOME-2 temperature-dependent absorption cross sections of O3 in the 231-794 nm range, Journal of Quantitative Spectroscopy and Radiative Transfer, 61, 509–517, https://doi.org/https://doi.org/10.1016/S0022-4073(98)00037-5, 1999.

Cachorro, V., Casanova, J., and de Frutos, A.: The influence of Angstrom parameters on calculated direct solar spectral irradiances at high turbidity, Solar Energy, 39, 399 – 407, https://doi.org/https://doi.org/10.1016/S0038-092X(87)80058-0, 1987.

Cachorro, V., Durán, P., and De Frutos, A.: Retrieval of vertical ozone content using the Chappuis band with high spectral resolution solar radiation measurements, Geophysical research letters, 23, 3325–3328, https://doi.org/https://doi.org/10.1029/96GL03239, 1996.

Cachorro, V. E., Durán, P., Vergaz, R., and de Frutos, A. M.: Measurements of the atmospheric turbidity of the north-centre continental area in Spain: Spectral aerosol optical depth and Ångström turbidity parameters, Journal of Aerosol Science, 31, 687–702, https://doi.org/https://doi.org/10.1016/S0021-8502(99)00552-2, 2000.

Cachorro, V. E., Berjøn, A., Toledano, C., Mogo, S., Prats, N., de Frutos, A. M., Vilaplana, J. M., Sorribas, M., De La Morena, B. A., Gröbner, J., and Laulainen, N.: Detailed Aerosol Optical Depth Intercomparison between Brewer and Li-Cor 1800 Spectroradiometers and a Cimel Sun Photometer, Journal of Atmospheric and Oceanic Technology, 26, 1558–1571, https://doi.org/10.1175/2009JTECHA1217.1, 2009.

Cuevas, E., Milford, C., Bustos, J. J., del Campo-Hernández, García, O., D., G. R., Gómez-Peláez, Guirado-Fuentes, C., Marrero, C., Prats, N., Ramos, R., Redondas, A., Reyes, E., Rodríguez, S., Romero-Campos, P., Scheneider, M., Belmonte, J., Yela, M., Almansa, F., Barreto, A., López-Solano, C., Basart, S., Terradellas, E., Afonso, S., Bayo, C., Berjón, A., Bethencourt, J., Carreño, V., Castro, N. J., Cruz, A. M., Damas, M., De Ory-Ajamil, F., García, M. I., Gómez-Trueba, V., González, Y., Hernández, C., Hernández, Y., Hernández-Cruz, B., Jover, M., León, S., López-Fernández, R., López-Solano, J., Rodríguez, E., Rodríguez-Franco, J., Rodríguez-Valido, M., Sálamo, C., Sanromá, E., Santana, D., Santo-Tomás, F., Sepúlveda, E., Sierra, M., and Sosa, E.: Izaña Atmospheric Research Center Activity Report 2015-2016, State Meteorological Agency (AEMET), 2017.

Cuevas, E., Romero-Campos, P. M., Kouremeti, N., Kazadzis, S., Räisänen, P., García, R. D., Barreto, A., Guirado-Fuentes, C., Ramos, R., Toledano, C., Almansa, F., and Gröbner, J.: Aerosol optical depth comparison between GAW-PFR and AERONET-Cimel radiometers from long-term (2005–2015) 1 min synchronous measurements, Atmospheric Measurement Techniques, 12, 4309–4337, https://doi.org/10.5194/amt-12-4309-2019, https://www.atmos-meas-tech.net/12/4309/2019/, 2019.

Eck, T., Holben, B., Reid, J., Dubovik, O., Smirnov, A., O'neill, N., Slutsker, I., and Kinne, S.: Wavelength dependence of the optical depth of biomass burning, urban, and desert dust aerosols, Journal of Geophysical Research: Atmospheres, 104, 31 333–31 349, https://doi.org/10.1029/1999JD900923, 1999.

Egli, L., Gröbner, J., Hülsen, G., Bachmann, L., Blumthaler, M., Dubard, J., Khazova, M., Kift, R., Hoogendijk, K., Serrano, A., Smedley, A., and Vilaplana, J.-M.: Quality assessment of solar UV irradiance measured with array spectroradiometers, Atmospheric Measurement Techniques, 9, 1553–1567, https://doi.org/10.5194/amt-9-1553-2016, https://www.atmos-meas-tech.net/9/1553/2016/, 2016.

Emde, C., Buras-Schnell, R., Kylling, A., Mayer, B., Gasteiger, J., Hamann, U., Kylling, J., Richter, B., Pause, C., Dowling, T., et al.: The libRadtran software package for radiative transfer calculations (version 2.0. 1), Geoscientific Model Development, pp. 1647–1672, https://doi.org/http://doi.org/10.5194/gmd-9-1647-2016, 2016.

Emilio, M., Kuhn, J. R., Bush, R. I., and Scholl, I. F.: Measuring the solar radious from space during the 2003 and 2006 mercury transits, The Astrophysical, 750, https://doi.org/10.1088/0004-637x/750/2/135, 2012.

Estellés, V., Utrillas, M., Martínez-Lozano, J., Alcántara, A., Alados-Arboledas, L., Olmo, F., Lorente, J., De Cabo, X., Cachorro, V., Horvath, H., et al.: Intercomparison of spectroradiometers and Sun photometers for the determination of the aerosol optical depth during the VELETA-2002 field campaign, Journal of Geophysical Research: Atmospheres, 111, https://doi.org/https://doi.org/10.1029/2005JD006047, 2006.

García, M. I., Rodríguez, S., and Alastuey, A.: Impact of North America on the aerosol composition in the North Atlantic free troposphere, Atmospheric Chemistry and Physics, 17, 7387–7404, https://doi.org/10.5194/acp-17-7387-2017, https://www.atmos-chem-phys.net/17/7387/2017/, 2017.

García, R. D., García, O. E., Cuevas, E., Cachorro, V. E., Romero-Campos, P. M., Ramos, R., and de Frutos, A. M.: Solar radiation measurements compared to simulations at the BSRN Izaña station. Mineral dust radiative forcing and efficiency study, Journal of Geophysical Research: Atmospheres, 119, 179–194, https://doi.org/doi:10.1002/2013JD020301, 2014.

Gasteiger, J., Emde, C., Mayer, B., Buras, R., Buehler, S., and Lemke, O.: Representative wavelengths absorption parameterization applied to satellite channels and spectral bands, Journal of Quantitative Spectroscopy and Radiative Transfer, 148, 99–115, https://doi.org/http://dx.doi.org/10.1016/j.jqsrt.2014.06.024, 2014.

Giles, D. M., Sinyuk, A., Sorokin, M. G., Schafer, J. S., Smirnov, A., Slutsker, I., Eck, T. F., Holben, B. N., Lewis, J. R., Campbell, J. R., Welton, E. J., Korkin, S. V., and Lyapustin, A. I.: Advancements in the Aerosol Robotic Network (AERONET) Version 3 database – automated near-real-time quality control algorithm with improved cloud screening for Sun photometer aerosol optical depth (AOD) measurements, Atmospheric Measurement Techniques, 12, 169–209, https://doi.org/10.5194/amt-12-169-2019, https://www.atmos-meas-tech.net/12/169/2019/, 2019.

Gröbner, J., Vergaz, R., Cachorro, V. E., Henriques, D., Lamb, K., Redondas, A., Vilaplana, J. M., and Rembges, D.: Intercomparison of aerosol optical depth measurements in the UVB using Brewer Spectrophotometers and a Li-Cor Spectrophotometer, Geophysical research letters, 28, 1691–1694, https://doi.org/https://doi.org/10.1029/2000GL012759, 2001.

Gueymard, C.: SMARTS2: a simple model of the atmospheric radiative transfer of sunshine: algorithms and performance assessment, Florida Solar Energy Center Cocoa, FL, 1995.

Gueymard, C. A.: Parameterized transmittance model for direct beam and circumsolar spectral irradiance, Solar Energy, 71, 325–346, https://doi.org/https://doi.org/10.1016/S0038-092X(01)00054-8, 2001.

Halthore, R. N., Schwartz, S. E., Michalsky, J. J., Anderson, G. P., Ferrare, R. A., Holben, B. N., and Ten Brink, H. M.: Comparison of model estimated and measured direct-normal solar irradiance, Journal of Geophysical Research: Atmospheres, 102, 29 991–30 002, https://doi.org/10.1029/97JD02628, 1997.

Hansen, J. E. and Travis, L. D.: Light scattering in planetary atmospheres, Space science reviews, 16, 527–610, https://doi.org/https://doi.org/10.1007/BF00168069, 1974.

Hess, M., Koepke, P., and Schult, I.: Optical properties of aerosols and clouds: The software package OPAC, Bulletin of the American meteorological society, 79, 831–844, https://doi.org/https://doi.org/10.1175/1520-0477(1998)079<0831:OPOAAC>2.0.CO;2, 1998.

Holben, B., Eck, T., Slutsker, I., Tanré, D., Buis, J., Setzer, A., Vermote, E., Reagan, J., Kaufman, Y., Nakajima, T., Lavenu, F., Jankowiak, I., and Smirnov, A.: AERONET—A Federated Instrument Network and Data Archive for Aerosol Characterization, Remote Sensing of Environment, 66, 1 – 16, https://doi.org/https://doi.org/10.1016/S0034-4257(98)00031-5, 1998.

Holben, B., Tanre, D., Smirnov, A., Eck, T., Slutsker, I., Abuhassan, N., Newcomb, W., Schafer, J., Chatenet, B., Lavenu, F., et al.: An emerging ground-based aerosol climatology: Aerosol optical depth from AERONET, Journal of Geophysical Research: Atmospheres, 106, 12 067–12 097, https://doi.org/https://doi.org/10.1029/2001JD900014, 2001.

IPCC: The Physical Science Basis. Intergovernmental Panel on Climate Change, https://doi.org/doi:10.1017/CBO9781107415324, 2013.

Kasten, F.: A new table and approximation formula for the relative optical air mass, Arch. Meteor. Geophy. B, 14, 206–223, 1966.

Kasten, F. and Young, A. T.: Revised optical air mass tables and approximation formula, Appl. Opt., 28, 4735–4738, https://doi.org/10.1364/AO.28.004735, 1989.

Kazadzis, S., Bais, A., Kouremeti, N., Gerasopoulos, E., Garane, K., Blumthaler, M., Schallhart, B., and Cede, A.: Direct spectral measurements with a Brewer spectroradiometer: absolute calibration and aerosol optical depth retrieval, Appl. Opt., 44, 1681–1690, https://doi.org/10.1364/AO.44.001681, 2005.

Kazadzis, S., Veselovskii, I., Amiridis, V., Gröbner, J., Suvorina, A., Nyeki, S., Gerasopoulos, E., Kouremeti, N., Taylor, M., Tsekeri, A., and Wehrli, C.: Aerosol microphysical retrievals from precision filter radiometer direct solar radiation measurements and comparison with AERONET, Atmospheric Measurement Techniques, 7, 2013–2025, https://doi.org/10.5194/amt-7-2013-2014, https://www.atmos-meas-tech.net/7/2013/2014/, 2014.

Kazadzis, S., Kouremeti, N., Diémoz, H., Gröbner, J., Forgan, B. W., Campanelli, M., Estellés, V., Lantz, K., Michalsky, J., Carlund, T., Cuevas, E., Toledano, C., Becker, R., Nyeki, S., Kosmopoulos, P. G., Tatsiankou, V., Vuilleumier, L., Denn, F. M., Ohkawara, N., Ijima, O., Goloub, P., Raptis, P. I., Milner, M., Behrens, K., Barreto, A., Martucci, G., Hall, E., Wendell, J., Fabbri, B. E., and Wehrli, C.: Results from the Fourth WMO Filter Radiometer Comparison for aerosol optical depth measurements, Atmospheric Chemistry and Physics, 18, 3185–3201, https://doi.org/10.5194/acp-18-3185-2018, 2018a.

Kazadzis, S., Kouremeti, N., Nyeki, S., Gröbner, J., and Wehrli, C.: The World Optical Depth Research and Calibration Center (WORCC) quality assurance and quality control of GAW-PFR AOD measurements, Geoscientific Instrumentation, Methods and Data Systems, 7, 39–53, https://doi.org/10.5194/gi-7-39-2018, 2018b.

Kiedron, P. W. and Michalsky, J. J.: Non-parametric and least squares Langley plot methods, Atmospheric Measurement Techniques, 9, 215–225, https://doi.org/10.5194/amt-9-215-2016, https://www.atmos-meas-tech.net/9/215/2016/, 2016.

Komhyr, W. D., Grass, R. D., and Leonard, R. K.: Dobson spectrophotometer 83: A standard for total ozone measurements, 1962–1987, Journal of Geophysical Research: Atmospheres, 94, 9847–9861, 1989.

Kurucz, R. L.: Synthetic infrared spectra, in: Infrared solar physics, pp. 523–531, Springer, 1994.

López-Solano, J., Redondas, A., Carlund, T., Rodriguez-Franco, J. J., Diémoz, H., León-Luis, S. F., Hernández-Cruz, B., Guirado-Fuentes, C., Kouremeti, N., Gröbner, J., Kazadzis, S., Carreño, V., Berjón, A., Santana-Díaz, D., Rodríguez-Valido, M., De Bock, V., Moreta, J. R., Rimmer, J., Smedley, A. R. D., Boulkelia, L., Jepsen, N., Eriksen, P., Bais, A. F., Shirotov, V., Vilaplana, J. M., Wilson, K. M., and Karppinen, T.: Aerosol optical depth in the European Brewer Network, Atmospheric Chemistry and Physics, 18, 3885–3902, https://doi.org/10.5194/acp-18-3885-2018, https://www.atmos-chem-phys.net/18/3885/2018/, 2018.

Major, G.: A method for determining the circumsolar sky function, Tellus, 32, 340–347, https://doi.org/https://doi.org/10.1111/j.2153-3490.1980.tb00961.x, 1980.

Mayer, B.: Radiative transfer in the cloudy atmosphere, in: EPJ Web of Conferences, vol. 1, pp. 75–99, EDP Sciences, https://doi.org/https://doi.org/10.1140/epjconf/e2009-00912-1, 2009.

Mayer, B. and Kylling, A.: Technical note: The libRadtran software package for radiative transfer calculations - description and examples of use, Atmospheric Chemistry and Physics, 5, 1855–1877, https://doi.org/10.5194/acp-5-1855-2005, https://www.atmos-chem-phys.net/5/1855/2005/, 2005.

Michalsky, J., Liljegren, J., and Harrison, L.: A comparison of sun photometer derivations of total column water vapor and ozone to standard measures of same at the Southern Great Plains Atmospheric Radiation Measurement site, Journal of Geophysical Research: Atmospheres, 100, 25 995–26 003, https://doi.org/https://doi.org/10.1029/95JD02706, 1995.

Neumann, A. and Witzke, A.: The influence of sunshape on the DLR solar furnace beam, Solar Energy, 66, 447–457, https://doi.org/https://doi.org/10.1016/S0038-092X(99)00048-1, 1999.

Pastiels, R.: Contribution à l'étude du problème des méthodes actinométriques, 1959.

Pierluissi, J. H. and Tsai, C.-M.: Molecular transmittance band model for oxygen in the visible, Applied optics, 25, 2458–2460, https://doi.org/https://doi.org/10.1364/AO.25.002458, 1986.

Pierluissi, J. H. and Tsai, C.-M.: New LOWTRAN models for the uniformly mixed gases, Applied optics, 26, 616–618, https://doi.org/https://doi.org/10.1364/AO.26.000616, 1987.

Pó, M., Hoogendijk, K., Beuttell, W., Kazunori, S., and Takeuchi, E.: Direct Spectral Irradiance Measurements from Rotating Shadowband EKO Grating Spectroradiometer, in: 2018 IEEE 7th World Conference on Photovoltaic Energy Conversion (WCPEC)(A Joint Conference of 45th IEEE PVSC, 28th PVSEC & 34th EU PVSEC), pp. 2337–2340, IEEE, https://doi.org/10.1109/PVSC.2018.8547445, 2018.

Räisänen, P. and Lindfors, A. V.: On the Computation of Apparent Direct Solar Radiation, Journal of the Atmospheric Sciences, 76, 2761–2780, https://doi.org/10.1175/JAS-D-19-0030.1, 2019.

Raptis, P.-I., Kazadzis, S., Gröbner, J., Kouremeti, N., Doppler, L., Becker, R., and Helmis, C.: Water vapour retrieval using the Precision Solar Spectroradiometer, Atmospheric Measurement Techniques, 11, 1143–1157, https://doi.org/10.5194/amt-11-1143-2018, https://www.atmos-meas-tech.net/11/1143/2018/, 2018.

Redondas, A., Nevas, S., Berjón, A., Sildoja, M.-M., León-Luis, S. F., Carreño, V., and Santana-Díaz, D.: Wavelength calibration of Brewer spectrophotometer using a tunable pulsed laser and implications to the Brewer ozone retrieval, Atmospheric Measurement Techniques, 11, 3759–3768, https://doi.org/10.5194/amt-11-3759-2018, https://www.atmos-meas-tech.net/11/3759/2018/, 2018.

Reinhardt, B.: On the retrieval of circumsolar radiation from satellite observations and weather model output, Ph.D. thesis, LMU München: Faculty of Physics, 2013.

Romero Campos, P. M., Cuevas Agulló, E., Ramos López, R., Valdés Pérez de Vargas, M., and Schneider, M.: Programa de vapor de agua en columna del Centro de Investigación Atmosférica de Izaña: Análisis e Intercomparación de diferentes Técnicas de Medida, NIPO 784-09-009-9, Agencia Estatal de Meteorologia, Ministerio de Medio Ambiente, y Medio Rural y Marino, 2009.

Rothman, L., Gordon, I., Babikov, Y., Barbe, A., Benner, D. C., Bernath, P., Birk, M., Bizzocchi, L., Boudon, V., Brown, L., Campargue, A., Chance, K., Cohen, E., Coudert, L., Devi, V., Drouin, B., Fayt, A., Flaud, J.-M., Gamache, R., Harrison, J., Hartmann, J.-M., Hill, C., Hodges, J., Jacquemart, D., Jolly, A., Lamouroux, J., Roy, R. L., Li, G., Long, D., Lyulin, O., Mackie, C., Massie, S., Mikhailenko, S., Müller, H., Naumenko, O., Nikitin, A., Orphal, J., Perevalov, V., Perrin, A., Polovtseva, E., Richard, C., Smith, M., Starikova, E., Sung, K., Tashkun, S., Tennyson, J., Toon, G., Tyuterev, V., and Wagner, G.: The HITRAN2012 molecular spectroscopic database, Journal of Quantitative Spectroscopy and Radiative Transfer, 130, 4–50, https://doi.org/https://doi.org/10.1016/j.jqsrt.2013.07.002, 2013.

Schmid, B., Michalsky, J., Halthore, R., Beauharnois, M., Harrison, L., Livingston, J., Russell, P., Holben, B., Eck, T., and Smirnov, A.: Comparison of aerosol optical depth from four solar radiometers during the fall 1997 ARM intensive observation period, Geophysical Research Letters, 26, 2725–2728, https://doi.org/10.1029/1999GL900513, https://agupubs.onlinelibrary.wiley.com/doi/abs/10.1029/1999GL900513, 1999.

Schmid, B., Michalsky, J., Slater, D., Barnard, J., Halthore, R., Liljegren, J., Holben, B., Eck, T., Livingston, J., Russell, Philip B.R., I. T., and I., S.: Comparison of columnar water-vapor measurements from solar transmittance methods, Applied Optics, 40, 1886–1896, https://doi.org/https://doi.org/10.1364/AO.40.001886, 2001.

Schneider, M., Blumenstock, T., Chipperfield, M. P., Hase, F., Kouker, W., Reddmann, T., Ruhnke, R., Cuevas, E., and Fischer, H.: Subtropical trace gas profiles determined by ground-based FTIR spectroscopy at Iza241;a (28deg; N, 16deg; W): Five-year record, error analysis, and comparison with 3-D CTMs, Atmospheric Chemistry and Physics, 5, 153–167, https://doi.org/10.5194/acp-5-153-2005, https://www.atmos-chem-phys.net/5/153/2005/, 2005.

Sengupta, M., Habte, A. M., Xie, Y., Lopez, A. J., Dooraghi, M., Kutchenreiter, M. C., Andreas, A. M., Reda, I. M., Maclaurin, G. J., Foster, M. J., and Gueymard, C.: Solar Resource Calibration, Measurement, and Dissemination: Final Report FY 2016-FY 2018, Tech. rep., National Renewable Energy Lab.(NREL), Golden, CO (United States), https://doi.org/10.2172/1513198, 2019.

Shaw, G. E.: Sun Photometry, Bulletin of the American Meteorological Society, 64, 4–10, https://doi.org/10.1175/1520-0477(1983)064<0004:SP>2.0.CO;2, 1983.

Shaw, G. E., Reagan, J. A., and Herman, B. M.: Investigations of atmospheric extinction using direct solar radiation measurements made with a multiple wavelength radiometer, Journal of Applied Meteorology, 12, 374–380, https://doi.org/10.1175/1520-0450(1973)012<0374:IOAEUD>2.0.CO;2, 1973.

Sinyuk, A., Holben, B. N., Smirnov, A., Eck, T. F., Slutsker, I., Schafer, J. S., Giles, D. M., and Sorokin, M.: Assessment of error in aerosol optical depth measured by AERONET due to aerosol forward scattering, Geophysical Research Letters, 39, https://doi.org/10.1029/2012GL053894, 2012.

Stamnes, K., Tsay, S.-C., Wiscombe, W., and Jayaweera, K.: Numerically stable algorithm for discrete-ordinate-method radiative transfer in multiple scattering and emitting layered media, Applied optics, 27, 2502–2509, https://doi.org/https://doi.org/10.1364/AO.27.002502, 1988.

Stamnes, K., Tsay, S.-C., Wiscombe, W., and Laszlo, I.: DISORT, a general-purpose Fortran program for discrete-ordinate-method radiative transfer in scattering and emitting layered media: documentation of methodology, Tech. rep., Tech. rep., Dept. of Physics and Engineering Physics, Stevens Institute of Technology, Hoboken, NJ 07030, 2000.

Takamura, T. and Nakajima, T.: Overview of SKYNET and its activities, Optica pura y aplicada, 37, 3303–3308, 2004.

Toledano, C., González, R., Fuertes, D., Cuevas, E., Eck, T. F., Kazadzis, S., Kouremeti, N., Gröbner, J., Goloub, P., Blarel, L., Román, R., Barreto, A., Berjón, A., Holben, B. N., and Cachorro, V. E.: Assessment of Sun photometer Langley calibration at the high-elevation sites Mauna Loa and Izaña, Atmospheric Chemistry and Physics, 18, 14 555–14 567, https://doi.org/10.5194/acp-18-14555-2018, 2018.

Vergaz, R., Cachorro, V. E., De Frutos, M., Vilaplana, J. M., and De La Morena, B. A.: Columnar characteristics of aerosols by spectroradiometer measurements in the maritime area of the Cadiz Gulf (Spain), International Journal of Climatology, 25, 1781–1804, https://doi.org/10.1002/joc.1208, 2005.

Wehrli, C.: Calibrations of filter radiometers for determination of atmospheric optical depth, Metrologia, 37, 419, http://stacks.iop.org/0026-1394/37/i=5/a=16, 2000.

Wehrli, C.: GAWPFR: A network of aerosol optical depth observations with precision filter radiometers, GLOBAL ATMOSPHERE WATCH, p. 36, 2005.

Wehrli, C.: Precision Filter Radiometer Documentation,Version 4.0, 38 pp.,Davos Dorf, 2008.

WMO: Recent progress in sunphotometry: determination of the aerosol optical depth, WMO/TD-No. 143; GAW Report-No. 43, 1986.

WMO: WMO/GAW Experts Workshop on a Global Surface-Based Network for Long Term Observations of Column Aerosol Optical Properties,GAW Report No. 162, WMO TD No. 1287, https://library.wmo.int/pmb_ged/wmo-td_1287.pdf, 2005.

WMO: Fourth WMO Workshop on the Impact of Various Observing Systems on Numerical Weather Prediction WMO/TD No. 1450, World Weather Watch, https://www.wmo.int/pages/prog/www/OSY/Meetings/NWP-4-Geneva2008/Abridged_Version.pdf(lastaccess: 14November2019), 2008.

WMO: Commission for Instruments and Methods of Observation,Sixteenth session WMO no.1138, Saint Petersburg,Secretariat of the World Meteorological Organization, 2014.

WMO: WMO/GAW Aerosol Measurement Procedures,Guidelines and Recommendations, 2nd Edition, WMO-No. 1177; GAW Report-No. 227, Guidelines and Recommendations, https://library.wmo.int/doc_num.php?explnum_id=3073, 2016.

Yoon, H. W., Sperfeld, P., Yousef, S. G., and Metzdorf, J.: NIST-PTB measurements of the radiometric temperatures of a high-temperature black body using filter radiometers, Metrologia, 37, 377, https://doi.org/10.1088/0026-1394/37/5/7, 2000.

Zong, Y., Brown, S. W., Johnson, B. C., Lykke, K. R., and Ohno, Y.: Simple spectral stray light correction method for array spectroradiometers, Appl. Opt., 45, 1111–1119, https://doi.org/10.1364/AO.45.001111, http://ao.osa.org/abstract.cfm?URI=ao-45-6-1111, 2006.